Hindawi
Advances in Materials Science and Engineering
Volume 2019, Article ID 8593193, 13 pages
https://doi.org/10.1155/2019/8593193

Research Article

Effect of Sterilization on the Properties of a Bioactive Hybrid Coating Containing Hydroxyapatite

E. K. K. Baldin,[1] **C. F. Malfatti**,[1] **V. Rodói**,[1] **and R. N. Brandalise**[2]

[1]*LAPEC, Federal University of Rio Grande do Sul (UFRGS), Bento Gonçalves Avenue, 9500 Porto Alegre, RS, Brazil*
[2]*PGPROTEC, University of Caxias do Sul (UCS), Francisco Getúlio Vargas Street, 1130 Caxias do Sul, RS, Brazil*

Correspondence should be addressed to E. K. K. Baldin; estelakerstner@gmail.com

Received 7 November 2018; Accepted 11 February 2019; Published 1 April 2019

Academic Editor: Michelina Catauro

The objective of this study was to evaluate the influence of sterilization on a hybrid coating obtained from a sol composed of alkoxysilane tetraethoxysilane (TEOS) and organoalkoxysilane methyltriethoxysilane (MTES) containing 10% (mass) of hydroxyapatite particles. The coating was obtained by dip coating, by applying two layers (protective/bioactive), which were cured at different temperatures (450°C and 60°C). The effects of sterilization on the superficial, electrochemical, bioactive, and mechanical properties of the coating were evaluated by performing different sterilization processes, namely, steam autoclave, hydrogen peroxide plasma, and ethylene oxide. Subsequently, the coating was characterized by using scanning electron microscopy (SEM/FEG), and FTIR measurements were performed to characterize the chemical structure. The bioactivity and degradability of the coating were analyzed by mass variation after immersion in SBF and X-ray diffraction (XRD) analysis. The electrochemical behavior was assessed by open circuit potential (OCP) and potentiodynamic polarization curves and the mechanical behavior by wear resistance. Results showed that all sterilization processes caused significant morphological changes in the hybrid coating. The autoclaved sample presented the highest structural chemical changes, and, consequently, the highest degradability, even though it had a superior bioactive behavior in relation to the other samples. In addition, the sterilization processes influenced the electrochemical behavior of the hybrid coating and altered the mechanical resistance to abrasion, thus presenting lower wear performance in relation to the nonsterilized sample.

1. Introduction

Titanium and its alloys are widely used as bone substitutes in the orthopedics and odontology areas due to their mechanical properties and cytocompatible behavior. However, they are materials with reduced capacity to stimulate the formation of new tissues. Numerous superficial treatments are proposed in order to improve their bioactivity [1–3], mainly by using materials considered osteoconductors.

Considering osteconductors, the application of bioactive coatings based on calcium phosphate, specifically hydroxyapatite [1], stands out. These materials are known to have the ability to react with physiological fluids, favoring the formation of an apatite layer that assists in the physical-chemical interaction between bone and implant [2]. Nevertheless, the use of only ceramic coatings is becoming restricted due to the poor adhesion of these to the metallic substrates, and the problems generated because of their mechanical properties [4, 5].

Thus, the application of bioactive coatings prepared by the sol-gel method on metallic substrates has been proved successful in the development of scientific research with application in biomaterials. This is due to the possibility of functionalization of these surfaces by the incorporation of particulate materials with osteoconductive properties [6–8]. Some researchers have used hybrid coatings based on organic-inorganic silicon precursors (silanes) [6, 7, 9]. These coatings consist of the combination of inorganic $Si(OR)_4$ and organic silanes $R'(CH_2)_nSi(OR)_3$, where R is a hydrolyzable alkoxy group and R' is an organofunctional group. They are formed by the occurrence of hydrolysis reactions and the condensation of the precursors, with the formation of a bonding network (Si–O–Si), uniform and chemically bound to the substrate [5, 8, 10].

Finally, being the last step that precedes the implantation of a biomaterial in the human body, the sterilization is also considered the last of the biomaterial superficial modifications. Its properties are affected as well, and, therefore, the process used must be carefully selected. Sterilization aims at eliminating all forms of microorganisms, including bacteria, spores, and fungi [11], thus, preventing the transmission of diseases and minimizing the incidence of infections [11, 12]. Some researchers have demonstrated the influence of sterilization processes on the properties of different biomaterials [12–14]. In this context, Walke et al. [15] showed the compromise of the corrosion resistance of a coating formed by TEOS and TMOS silanes on stainless steel (316L). Baldin et al. [16] observed that different sterilization processes caused alterations in the electrochemical properties and biocompatibility behavior with MG-63 cells for the silane coating composed of TEOS and MTES applied on the Ti6Al4V alloy. However, there is a lack of studies on the influence of sterilization on the osseointegration process for hybrid bioactive silane coatings.

The objective of this study is to evaluate the influence of different sterilization processes (steam autoclave, hydrogen peroxide plasma, and ethylene oxide) on the bioactivity, as well as on the morphological, electrochemical, and mechanical properties of a hybrid coating obtained from a sol consisting of alkoxysilane precursors, tetraethoxysilane (TEOS), and organoalkoxysilane methyltriethoxysilane (MTES) containing bioactive hydroxyapatite ceramic particles. This bioactive coating was applied on a hybrid coating of similar composition, but with protective properties to the Ti6Al4V alloy.

2. Materials and Methods

Figure 1 shows the flowchart of this study development. Step A contemplates the operations of obtaining the hybrid coating; step B presents the sterilization processes applied; and step C, the techniques used to characterize the coatings before and after the sterilization processes.

2.1. Obtaining the Hybrid Coating with Hydroxyapatite Particles. The hybrid coating was obtained by the synthesis of silane precursors, alkoxysilane tetraethoxysilane (TEOS), and organoalkoxysilane methyltriethoxysilane (MTES) (Sigma-Aldrich, 98%), 40 : 60 molar in ethyl alcohol, nitric acid (Neon, 66.2%), and acetic acid (Neon, 98%). They were in the following ratios: silane : water (1 : 2); water : ethyl alcohol (1 : 1); and water : acetic acid (7 : 1) [7, 17–20] in the nitric acid medium (pH ≈ 2). After 24 hours of hydrolysis of the TEOS/MTES precursors, the hydroxyapatite particles Sigma-Aldrich 90% were added in the proportion of 10% (mass) [19, 21]. The homogenization of the suspension was performed in a high shear mixer model 550 (Sonics), with a 40% amplitude during 6 minutes. This suspension was subsequently agitated for 24 hours until the deposition of the hybrid coating on a metallic substrate of Ti6Al4V, already coated with a protective coating, was obtained, according to the methodology by Baldin et al. [16].

The deposition of the coating was performed by the dip-coating technique (Marconi, Brazil), with the application of a single layer of sol, with velocities of entrance and withdrawal of the suspension of 18 cm·min^{-1} and immersion time of 5 minutes [7]. Subsequently, it was cured in a furnace (Sanchis, Brazil) at 60°C for 1 hour, with a heating rate of 10°C·min^{-1}.

2.2. Sterilization Processes. The sterilization of the hybrid coating was performed using three different processes: ethylene oxide, steam autoclave, and hydrogen peroxide plasma.

The sterilization in saturated steam and ethylene oxide autoclaves were performed at Esterilizare (a company in Caxias do Sul, Brazil) under the following conditions: autoclave (Baumer, series 050500001, HI-VAC Plus Autoclave Horizontal model) with a capacity of 0.56 m^3, at 134°C, pressure of 0.70 atm for 7 minutes of exposure; and ethylene oxide at a pressure of 0.65 atm, at temperature of 55°C, and for 180 minutes with gas (Chemogas) composed of 90% ethylene oxide and 10% carbon dioxide.

Plasma sterilization of hydrogen peroxide was performed at the Pompéia Hospital Sterile Processing Department (Caxias do Sul, Brazil) by using the Sterrad NX (Johnson and Johnson) sterilizer for 28 minutes. The temperature during the sterilization cycle ranged between 45 and 55°C. The parameters used for sterilization were those usually used in establishments (certified by ANVISA), without any modification to the process.

2.3. Characterization of Coatings before and after Sterilization

2.3.1. Physical-Chemical and Surface Properties. The hydrolyzed solutions, the hydroxyapatite particles, and the coating, before and after the sterilization processes, were characterized by Fourier transform infrared (FTIR) spectroscopy in attenuated total reflection (ATR), in the region between 4000 and 400 cm^{-1}, with 4 cm^{-1} resolution in the Nicolet IS10 spectrometer (Thermo Fisher Scientific, Wisconsin, USA).

The morphologies of the hydroxyapatite particles and the coating, before and after the sterilization processes and after the bioactivity experiments, were observed in top view using the Field Emission Gun Scanning Electron Microscopy (SEM/FEG) (Tescan Mira3, Czech Republic). Elemental mapping was carried out by X-Max (Oxford Instruments, United Kingdom) with dispersive energy spectroscopy (EDS) coupled to the high-resolution scanning microscope.

The adhesion of the hybrid coating on the protective coating was analyzed by the adaptation of the crosshatch and tape pull test, according to the ASTM D-3359-09 standard. For this, vertical and horizontal cuts were manually made on the deposited coating, and, subsequently, an adhesive tape was applied and pressed on it. Afterwards, the tape was removed with a slope near 180°, and the coating peel off was analyzed using SEM/FEG. The degree of adhesion was attributed to the amount of material removed from the coating beyond the marked areas. The micrometer roughness was

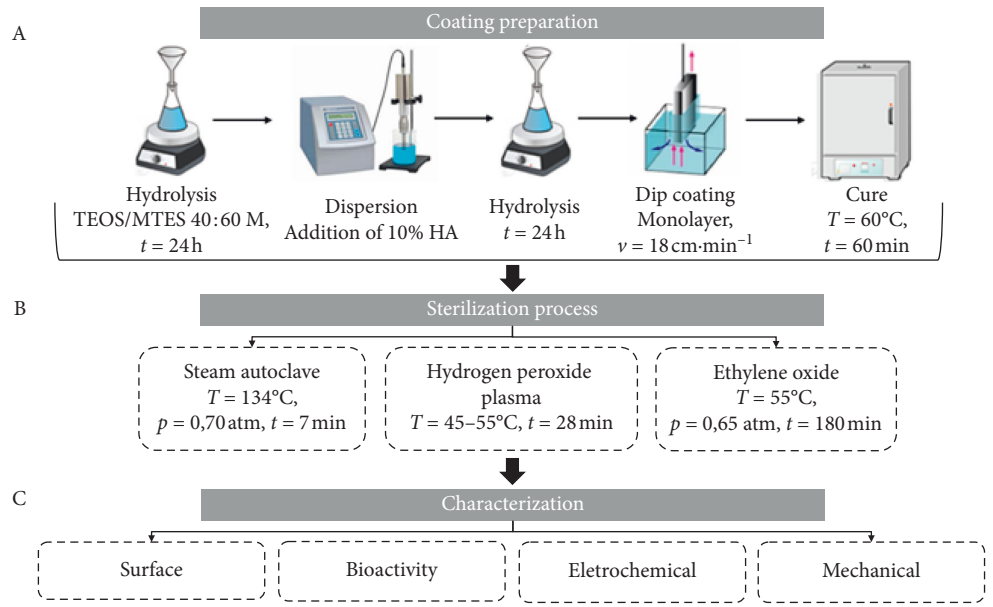

Figure 1: Flowchart of the development stages of this study.

analyzed in a surface roughness tester model Surftest SJ-301 (Mitutoyo, Japan) with cutoff of 0.08 mm.

The contact angle measurements, used to determine the surface wettability, were performed by the sessile drop method using an equipment developed by the Corrosion Research Laboratory (LAPEC) of the Federal University of Rio Grande do Sul (Porto Alegre, Brazil), in which a drop of the liquid was deposited on the surface using a micropipette. The drop was observed through a low magnification lens and the contact angle measured with a goniometer. The contact angle measurements were performed with a simulated body fluid solution (SBF). The SBF solution was prepared according to the methodology proposed by Kokubo and Takadama [22].

2.3.2. Bioactivity. The bioactive behavior of the coating was analyzed by immersing the samples in SBF at a temperature of approximately 37 ± 3°C for different evaluation times (24, 168, 336, and 672 hours) [9, 22]. After the termination of the selected times, the samples were removed from the solutions, washed with deionized water and dried in an oven at 37 ± 3°C for 48 hours. After, samples were weighed and the percentage of the mass variation was calculated. X-ray diffraction (XRD) analysis was also performed using Philips X'Pert MPD equipped with curved graphite monochromator and fixed copper anode, operating at 40 kV and 40 mA, with angles ranging from 5 to 75°, and a step of 5°·1 s^{-1}.

2.3.3. Electrochemical Properties. The electrochemical properties were determined by monitoring the open circuit potential (OCP) and the potentiodynamic polarization curves. Measurements were performed in a nonagitated medium, naturally aerated, at a temperature of approximately 37 ± 3°C, and an electrolyte of SBF, after 1 and 672 hours of immersion. A conventional three-electrode cell was used in the analyzes, being the saturated calomel (ECS) the reference electrode and the platinum the counter electrode interconnected to a potentiostat/galvanostat (Ivium-Stat of Ivium Technologies, Netherlands). The scanning interval was −200 mV below the open circuit potential, and 800 mV above it, with a scanning speed of 1 mV·s^{-1} [23, 24].

2.3.4. Mechanical Properties. The wear resistance tribological tests were performed using a UMT-3 tribometer (CETR, USA) with a computer-controlled ball-on-plate configuration. This test was performed in triplicate and 5 mm yttria-stabilized-zirconia (YSZ) balls were used as the counterbody, in linear and reciprocating movements. A load of 0.3 N was used for 60 minutes at a frequency of 1 Hz and 2 mm of track length.

Table 1 shows the names and descriptions used for the samples during this study.

3. Results and Discussion

3.1. Silane Hybrid Coating. Figure 2 shows the FTIR spectra of the TEOS/MTES solution after 24 hours of hydrolysis, of the solution after 48 hours with 24 hours of dispersion of the hydroxyapatite particles, and of the coating after curing at 60°C.

According to the mechanism for obtaining hybrid coatings by using the sol-gel method [25], the wide band ranging from 3200 to 3700 cm^{-1} in the spectrum obtained for the TEOS/MTES solution after 24 hours of hydrolysis can be attributed to the O-H bond due to the presence of the solvents, in which water and alcohol used in their synthesis. This bond can also be attributed to the formation Si-OH groups, evidenced by the appearance of the band between 800 and 890 cm^{-1}. The presence of the acetic acid catalyst was also verified due to the appearance of the band at

Table 1: Naming and description of the samples of this study.

Ti6Al4V/TM/TM_{HA}	Ti6Al4V sanded with protective coating application composed of TEOS and MTES cured at 450°C, and a second hybrid coating composed of TEOS and MTES containing 10% hydroxyapatite cured at 60°C
Ti6Al4V/TM/$TM_{HA/OE}$	Ti6Al4V sanded with protective coating application composed of TEOS and MTES cured at 450°C, and a hybrid coating containing 10% hydroxyapatite cured at 60°C, sterilized by the ethylene oxide process
Ti6Al4V/TM/$TM_{HA/AC}$	Ti6Al4V sanded with protective coating application composed of TEOS and MTES cured at 450°C, and hybrid coating composed of TEOS and MTES containing 10% hydroxyapatite cured at 60°C, sterilized by the autoclave process
Ti6Al4V/TM/$TM_{HA/PH}$	Ti6Al4V sanded with protective coating application composed of TEOS and MTES cured at 450°C, and a hybrid coating composed of TEOS and MTES containing 10% hydroxyapatite cured at 60°C, sterilized by the hydrogen peroxide plasma process

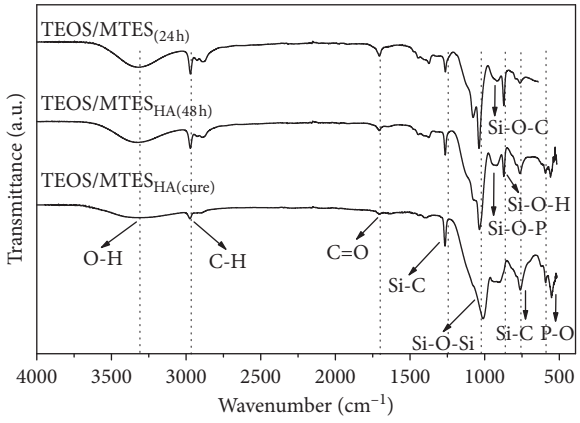

Figure 2: FTIR of the TEOS/MTES solution hydrolyzed for 24 h with the addition of the hydroxyapatite particles after 24 h and after condensation and cure stage.

approximately 1716 cm^{-1}, which refers to the stretching of the C=O bond. The absorbance at about 2900 cm^{-1} can be associated with the C–H bonds and symmetric and asymmetric (CH_2 and CH_3) stretches in the aliphatic alkoxysilane (TEOS) and organoalkoxysilane (MTES) chains. Moreover, the band located at 958 cm^{-1} may be associated with the asymmetric stretching of PO_4^{-3} present in the chemical structure of hydroxyapatite [25–27].

The infrared spectrum obtained after 48 hours of solution hydrolysis, during which there were 24 hours of dispersion of the hydroxyapatite particles, revealed the formation of the Si–O–P chemical bonds by the appearance of the band located near 876 cm^{-1}, which results from reaction of the hydroxyl groups present in the structure of hydroxyapatite with those present in the silanol group [28–30]. The formation of this bond can also be confirmed by the lower intensity of the bands related to the Si–OH bond, when these are compared to the spectrum obtained after 24 hours of hydrolysis. According to Mora et al. [31], the occurrence of covalent bonds with particles dispersed in the sol-gel network may favor the formation of crosslinks, causing a greater densification of the final coating.

Finally, after 60 minutes of curing at 60°C, the reaction of condensation between the silanol groups with the formation of the siloxane (Si–O–Si) bonds was observed, being evidenced by the appearance of a band at approximately 1020 cm^{-1}. In addition, the bands were associated with the C–H (CH_2 and CH_3), and Si–C (Si–CH_3) bonds were present in the lateral grouping of the organoalkoxysilane MTES, and the O–H bond band was also observed. The retention of the water and/or the permanence of the silanol groups (between 3200 and 3700 cm^{-1}) were observed even after the curing step.

According to Hernández-Escalano et al. [32], the curing temperature used to obtain the silane coatings may influence their properties. Usually, higher temperatures are used to obtain coatings for improving the corrosion resistance of metal substrates, and lower temperatures are used in the biomedical area to provide these coatings with osteoconductive properties. The curing temperature of 60°C was chosen because, according to Latifi et al. [33], the presence of hydroxyls in these coatings tends to favor bioactivity since they provide the highest nucleation and growth of apatite. Thus, from the observation of such groups in the FTIR spectra of the cured hybrid coating, this would be the coating proposed for application in the area of biomaterials.

In addition, the silane hybrid coating can also be confirmed by the images obtained in EDS due to the detection of the main chemical constituents of the siloxane (Si−O−Si): silicon and oxygen bonds, together with the elements of the structure of hydroxyapatite, calcium, and phosphorus. Based on the micrographs obtained from the SEM/FEG experiments, the adhesion of the silane hybrid coating containing hydroxyapatite particles can be evidenced since their removal occurred only in small regions which were not in those previously marked. Such adhesion can be observed by their satisfactory interaction in Figure 3(B). The layer thickness obtained was of approximately 1.1 μm, corroborating the results published by Ballarre et al. [19], who used the same silicon precursors but applied on an AISI 316L substrate.

3.2. Effect of Sterilization Processes on Silane Hybrid Coating

3.2.1. Surface Properties. Figure 4 shows the micrographs of the hybrid silane coating before and after the different sterilization processes.

In the micrographs, the deposition of a homogeneous coating, which was defect-free and with hydroxyapatite particles uniformly distributed throughout the surface but covered by the coating, was observed. In the literature, the use of the sol-gel method is indicated for incorporation of particles in order to obtain homogeneous coatings for functionalization of different surfaces [34]. On the contrary,

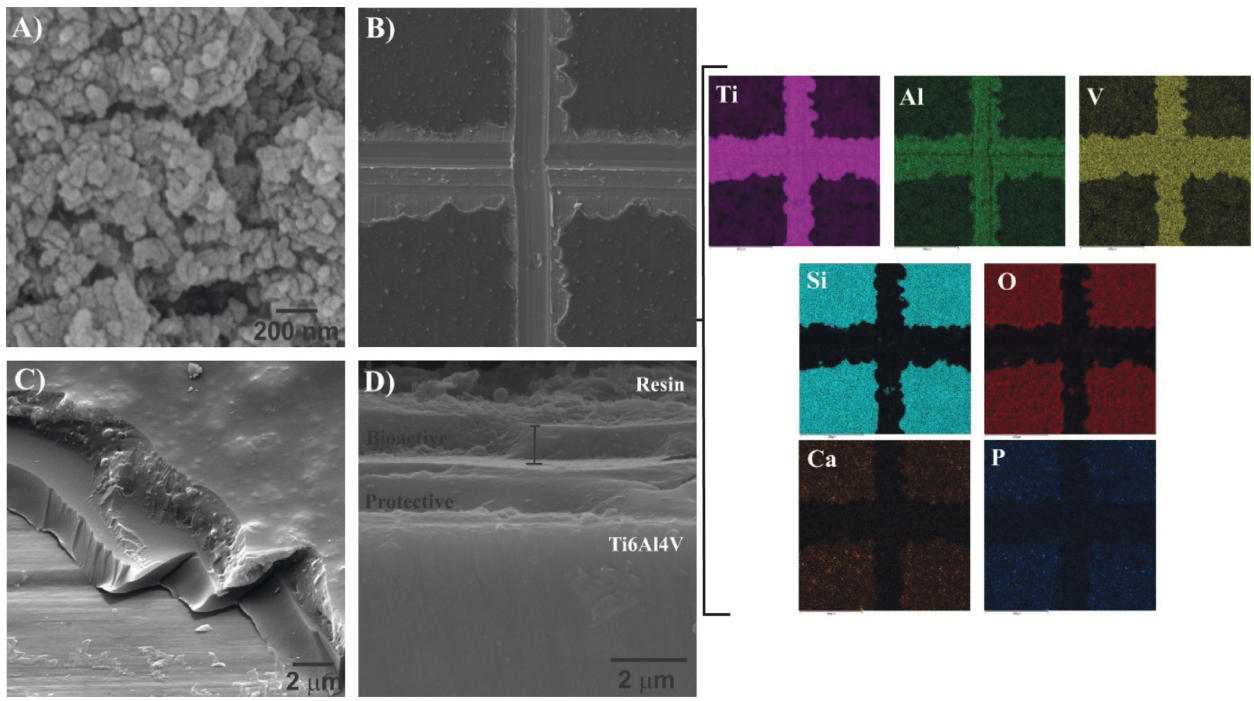

Figure 3: SEM/FEG micrographs (A) of the hydroxyapatite particles and the hybrid coating cured at 60°C in different analyzed areas, (B) after the adhesion assay with elemental mapping according to the coating composition, (C) of the detachment region with slope of 35°, and (D) of the transverse view of deposited coating.

according to Mora et al. [31], the presence of agglomerated particles tends to negatively influence the mechanical properties of these coatings. After sterilization, all the processes to have modified the morphology of the hybrid coating, as well as increased the layer thickness, thus producing a completely porous material in the bulk, although less porous on the surface. These changes could also be evidenced by the increase in the parameters of micrometric roughness of the sterilized samples in relation to the nonsterilized samples (Table 2). The Ti6Al4V/TM/$TM_{HA/AC}$ sample showed the highest surface exposure of the hydroxyapatite particles and, as a consequence, presented a higher surface roughness when compared to the other samples ($Ra = 0.44\,\mu m$). For the Ti6Al4V/TM/$TM_{HA/PH}$ sample, less significant morphological changes, and, consequently, values of the surface roughness parameters closer to the ones of the nonsterilized sample ($Ra = 0.24\,\mu m$) were observed. However, the adhesion behavior between the coatings (protective and bioactive), as well as the integrity of the deposited layer, was not evidenced (Figure 4).

Figure 5 shows the FTIR spectra and the mean contact angle values for the coating before and after the sterilization processes were carried out.

The sterilization processes modified the chemical structure of the coatings. Changes in the FTIR spectra (Figure 5), when compared to the nonsterilized sample, were seen. These were, mainly, seen in the reduction of the intensity of the bands at 3000, 3600 cm^{-1}, and 2900 cm^{-1}, which are attributed to the stretching of O–H and C–H bonds, to water retention, and/or the presence of the silanol group, and to the CH_3 bond of the MTES side group, respectively. These changes may be related to the increase of heating, which causes an increase in the temperature during sterilization and may have led to a greater crosslinking of these coatings. In addition, the Ti6Al4V/TM/$TM_{HA/AC}$ sample presented these modifications in greater intensity, which may be justified by the sensitization of the CH_3 groups to the pressure employed during this process [35].

The increase in the wettability of the sterilized coatings in relation to the nonsterilized coatings, as shown in Table 2, can be related to the chemical changes observed in the FTIR analysis (Figure 5). The reduction of the density of CH_3 groups compared to the hydroxyl groups has an important influence by increasing the hydrophilic behavior [17] of the sterilized hybrid coatings. Similar results were published by Wittenburg et al. [36] and Han et al. [37] when glass and zirconia surfaces were sterilized using similar processes.

The highest contact angle values were found for the autoclaved samples, followed by the samples sterilized with ethylene oxide, and hydrogen peroxide plasma. Therefore, it is possible to correlate the wettability and surface roughness results obtained after sterilization to Wenzel's theory by Pegueroles et al. [38] where it was affirmed that the increase in the roughness of a surface tends to cause a decrease in the values of contact angles due to the increased surface area.

3.2.2. Bioactivity. The correlation of the results obtained in XRD (Figure 6), mass variation (Figure 7), and SEM/FEG micrographs after 24 and 672 hours of immersion of the hybrid coatings in SBF (Figure 8) allowed the verification of

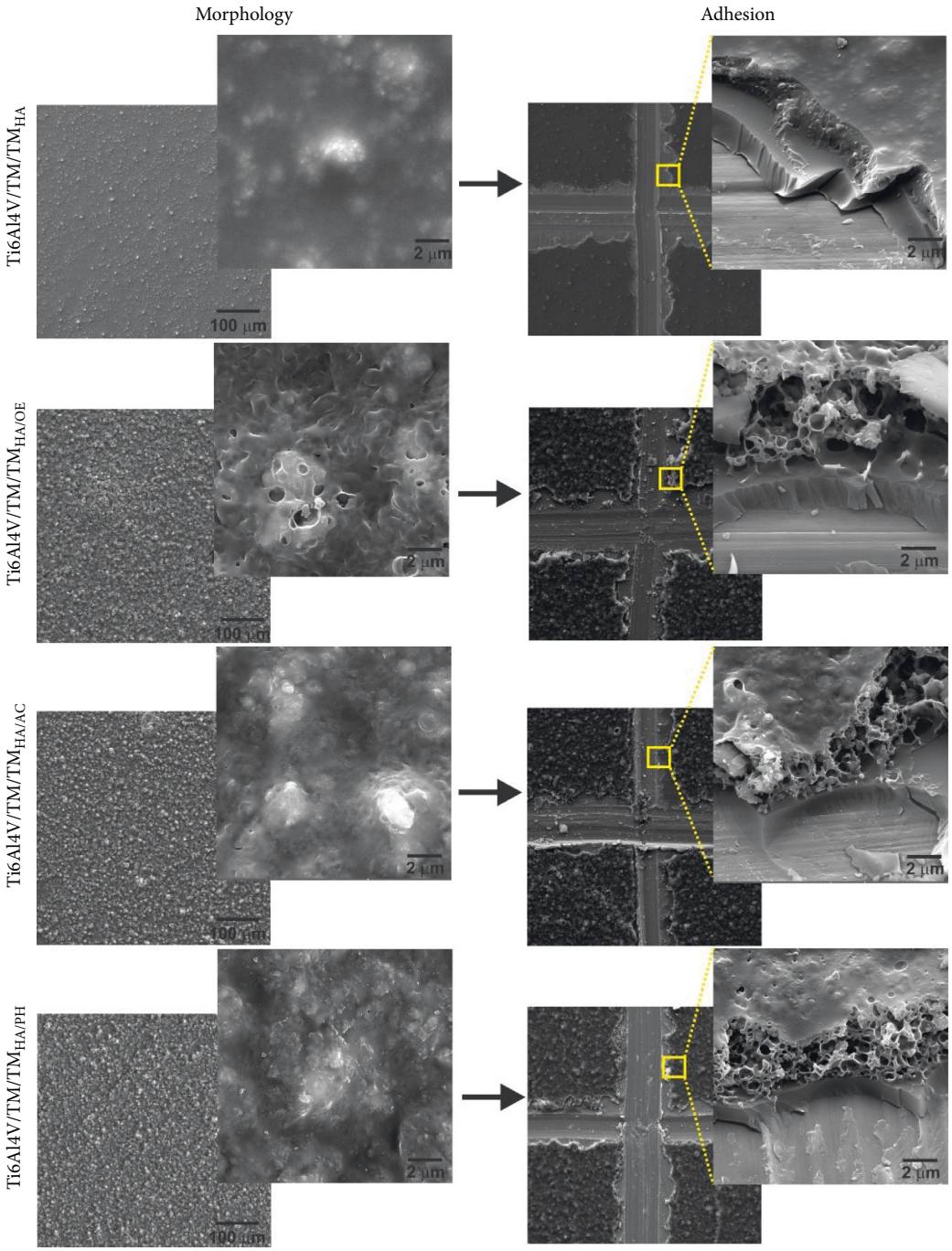

Figure 4: SEM/FEG micrographs of the nonsterilized and the sterilized (by three different processes) hybrid coatings before and after the adhesion test on the protective coating.

the influence of the sterilization processes on the composition and on the structure of the coatings, thus relating them with the bioactivity behavior.

Based on the analysis of the diffractograms, the peaks corresponding to the α and β phases, which belong to the metallic substrate of Ti6Al4V, were close to 40, 53, and 63° and to 36, 57, and 71°, respectively [39]. Similarly, the crystal structure of the hydroxyapatite particles incorporated in the coating was confirmed by detecting the peak near 26° (HA) [5]. In addition, after 672 hours, the relative intensity of the peaks close to 32 and 34°, which are related to the presence of amorphous hydroxyapatite (aHA) [18] and to the reduction of intensity of SiO_2 amorphous structure (TEOS/MTES) [40, 41] were compared to the Ti6Al4V peaks (α and β phases).

Regardless of the sterilization process used, the bioactivity behavior of the proposed coating was verified (Figures 6 and 7). This bioactive behavior was most likely due to the permeability of the electrolyte in the coatings, causing the instability of the siloxane bond network formed

Table 2: Mean values of roughness in the micrometric scale determined by contact profilometry for the nonsterilized and the sterilized (by three different processes) coatings.

Sample	Ra (μm)	Contact angle (°)
Ti6Al4V/TM/TM_{HA}	0.22 ± 0.03	81 ± 0.2
Ti6Al4V/TM/$TM_{HA/OE}$	0.39 ± 0.02	72 ± 0.7
Ti6Al4V/TM/$TM_{HA/AC}$	0.44 ± 0.04	64 ± 0.5
Ti6Al4V/TM/$TM_{HA/PH}$	0.24 ± 0.02	74 ± 0.5

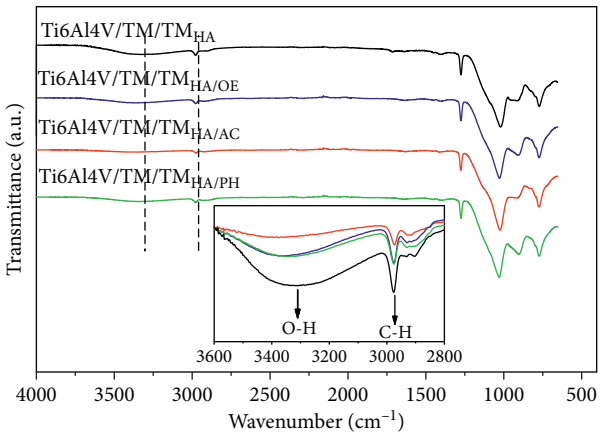

Figure 5: FTIR of the nonsterilized and the sterilized (by three different processes) hybrid coatings.

(reduction of the SiO_2 amorphous structure) and thereafter dissolving the hydroxyapatite particles dispersed in the coatings. These particles, when in contact with the SBF solution, triggered the formation of amorphous apatite on them (greater intensity of the peaks related to aHA, according to Ballarre et al. [18]). In addition, the increase in the mass percentages as a function of the analysis, as shown in Figure 7, corroborates the bioactive behavior of the coatings previously discussed.

The bioactive mechanism of a surface, according to the literature, occurs when the Ca^{+2} and PO_4^{-3} ions present in SBF react with the hydroxyl groups, inducing the nucleation of apatite (Reaction 2) [42]. Once nucleated, it tends to grow spontaneously and form the amorphous calcium phosphate, which is later deposited on the biomaterial [43–45]:

$$\begin{aligned} (SiO_2)_n + 2H_2O &\longrightarrow (SiO_2)_{n-1} + Si(OH)_4 \\ 5Ca^{+2} + 3PO_4^{-3} + OH^- &\longrightarrow Ca_5(PO_4)_3(OH) \end{aligned} \quad (1)$$

Zheng et al. [46] observed that the sol-gel silane coatings, which are effective for corrosion protection, applied on the nitinol alloy (NiTi) exhibited adequate bioactivity as a consequence of the presence of hydroxyl groups in it. Hydroxyls, in addition to the ones present in the chemical structure of the coating after curing and sterilization, can be formed from the hydrolytic hydrolysis of the Si–O–Si bonds (Reaction 1) [33], favoring the nucleation of apatite of calcium and or even of a mineralized matrix. In Ballarre et al. [18], the combination of the use of ceramic particles together with the dissolution of silane coatings is considered an important factor for the osseointegration process around metal implants.

The gain of mass presented by the nonsterilized sample after 24 and 168 hours of immersion suggests an advanced bioactive stage of this coating when compared to the other samples. Such behavior resembles that found by Tan et al. [47] since the authors suggested that a greater amount of OH available in the coating tends to promote faster precipitation of apatite. Additionally, the lower bioactive behavior for the sterilized samples in the first moment may be related to both lower hydroxyl numbers (Figure 5) and greater crosslinking observed, thus provoking a higher stability of the siloxane network formed.

Furthermore, according to Heise et al. [48], rough surfaces tend to promote increased nucleation and formation of apatite (aHA) when immersed in SBF, for instance, the Ti6Al4V/TM/$TM_{HA/AC}$ (51%) and Ti6Al4V/TM/$TM_{HA/PH}$ (38%) samples, when compared to the Ti6Al4V/TM/$TM_{HA/OE}$ (35%) and Ti6Al4V/TM/TM_{HA} (25%) samples after 672 hours of immersion. In addition, the higher wettability presented by Ti6Al4V/TM/$TM_{HA/AC}$ may also have influenced the hydrolytic degradation of this coating, thus contributing to its superior bioactive behavior in comparison with other samples [33, 49].

Moreover, for promoting *in vivo* bioactivity, the formation of apatite on the biomaterial can accelerate the biological processes that guide the formation of new bone, such as cell differentiation in osteoblasts, alkaline phosphatase activity, and extracellular matrix mineralization [22, 50].

After analyzing the SEM/FEG images (Figure 7) of the sample after 672 hours of immersion, regardless of the sterilization process, the surface defects were minimized if compared to the sample after 24 hours of immersion, hence confirming the bioactivity of the proposed coatings.

3.2.3. Electrochemical Properties. Figure 9 shows the measurements of the open circuit potential (OCP) monitoring and potentiodynamic polarization curves after 1 hour and 672 hours of immersion in SBF sterilized coating.

Up to approximately 360 hours of immersion, the potentials of the nonsterilized coating (bioactive + protective layer) were observed in more positive directions in relation to the sterilized samples (Figure 9(a)). In the same way, in the polarization curves obtained after 1 hour of immersion was observed the development of higher current densities of sterilized samples compared to the nonsterile sample (Figure 9(b)). These behaviors may be related to morphology since greater internal porosity (shown in Figure 4) coupled with higher wettability (Table 2) presented by these coatings after sterilization may have allowed a greater permeability of the electrolyte in it. This may be related to what has already been evidenced by Hosseinalipour et al. [51] when evaluating the electrochemical behavior of a stainless steel substrate (AISI 316L) coated with TEOS and TMOS hybrid films in different proportions. Besides, the superior bioactivity presented by the nonsterilized sample, at the same time of immersion in SBF (Figure 7), may have also contributed to this behavior since the apatite layer formed may have acted as a new physical barrier to the action of the electrolyte during the first moments of immersion. Consequently, at one hour of immersion, this sample developed lower current density values.

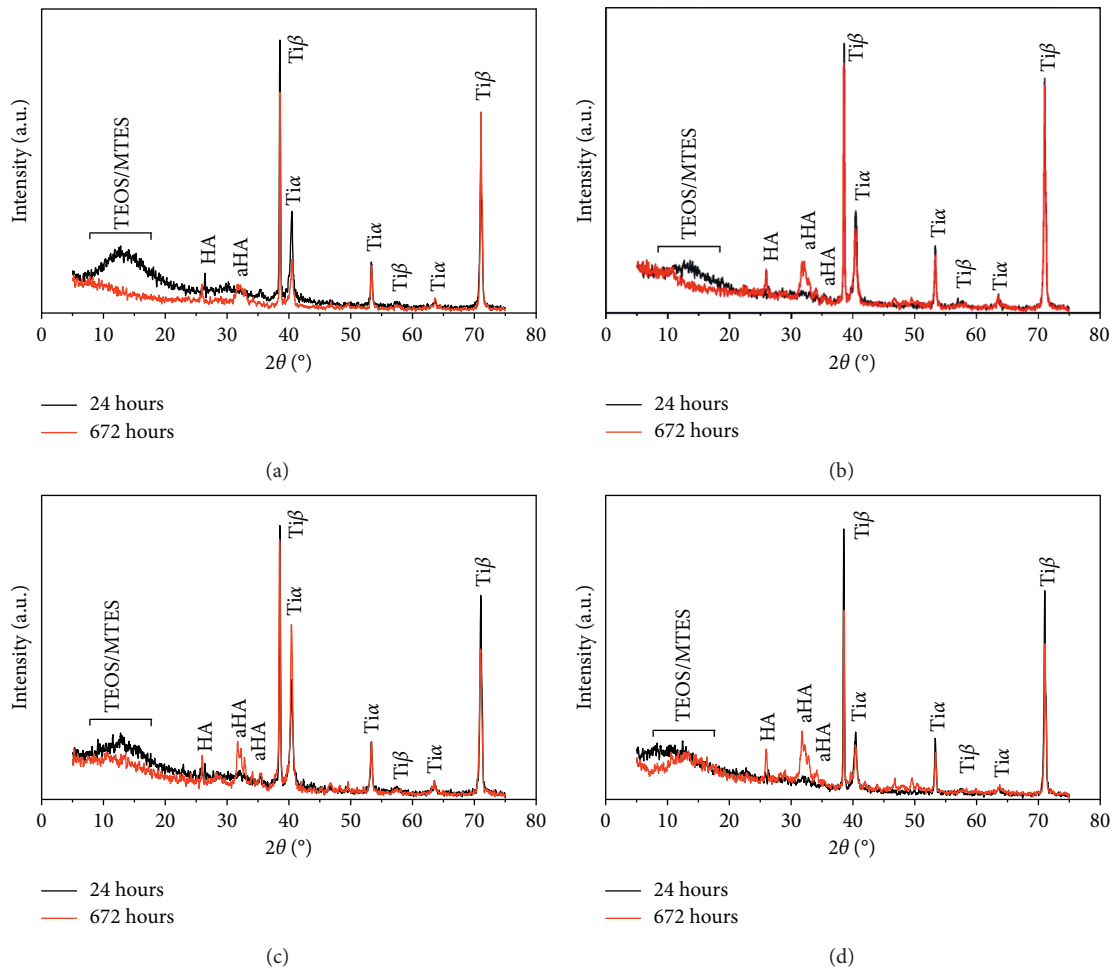

FIGURE 6: DRX of the coating before and after sterilization immersed for 24 and 672 hours in SBF at 37 ± 3°C: (a) Ti6Al4V/TM/TM_{HA}, (b) Ti6Al4V/TM/$TM_{HA/OE}$, (c) Ti6Al4V/TM/$TM_{HA/AC}$, and (d) Ti6Al4V/TM/$TM_{HA/PH}$.

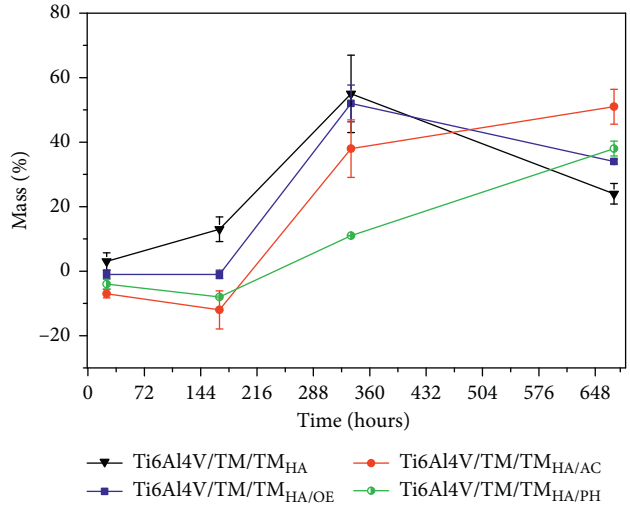

FIGURE 7: Variation of mass as a function of the time of the nonsterilized and the sterilized (by three different processes) coatings immersed for 24, 168, 336, and 672 hours in SBF at 37 ± 3°C.

However, after 672 hours of immersion in the anodic polarization assay, the sterilized samples developed lower current density, except for those sterilized with ethylene oxide. This may be associated with higher electrolyte permeability in these sterilized samples, which allowed the electrolyte to reach the substrate, and the formation of

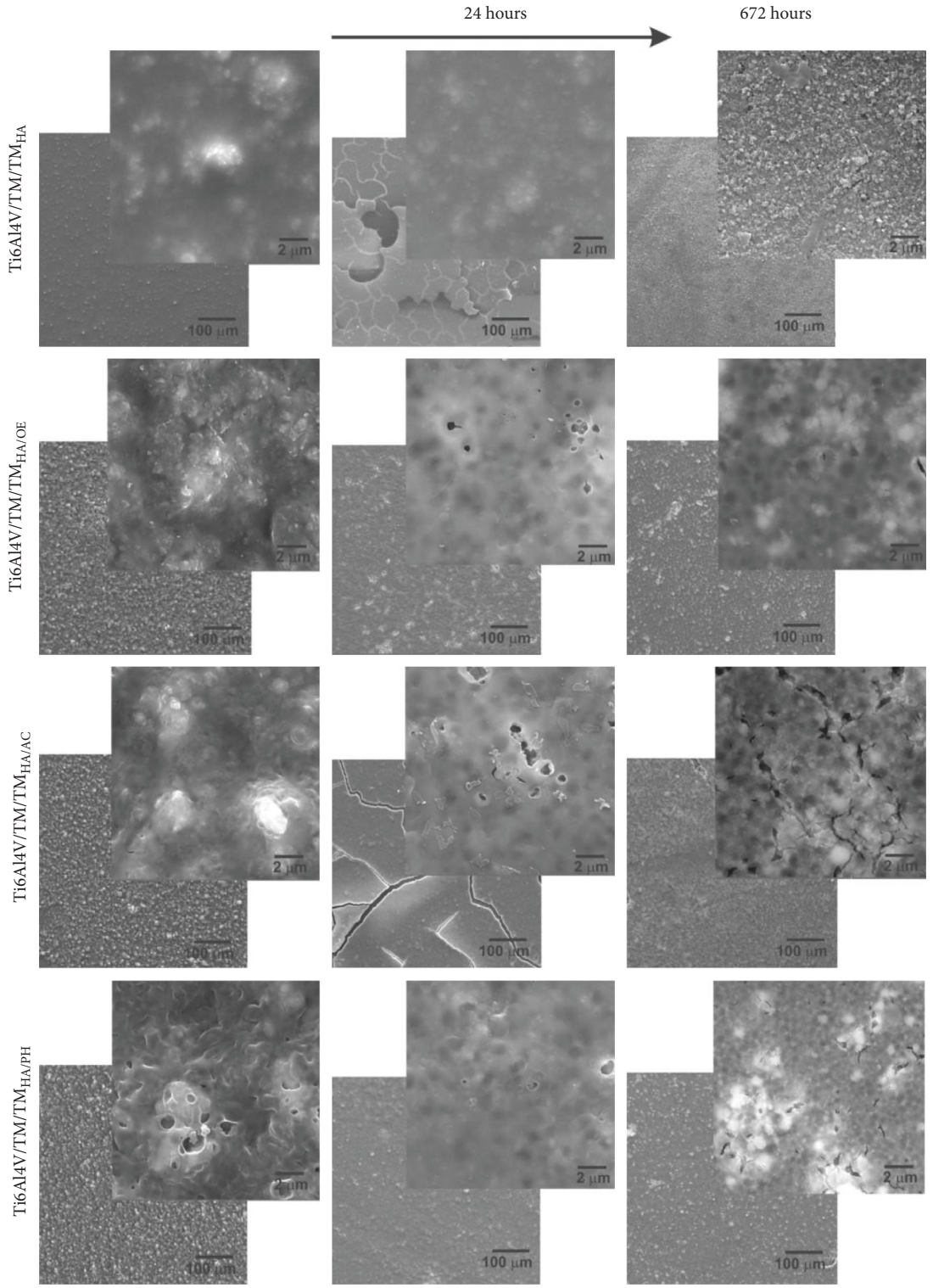

Figure 8: SEM/FEG micrographs of the nonsterilized and the sterilized (by three different processes) coatings immersed for 24 and 672 hours in SBF at 37 ± 3°C.

corrosion products consequently reduced the current densities developed by these systems.

Authors have reported the reduction of corrosion resistance over time for silane coatings due to higher rate of dissolution of bioactive particles, when compared to the rate of deposition of amorphous hydroxyapatite, causing the creation of preferential defects that facilitate the permeability of the electrolyte [8, 48]. The degradation of all the hybrid coatings observed in the present work, regardless of the sterilization process, can also be evidenced by comparing

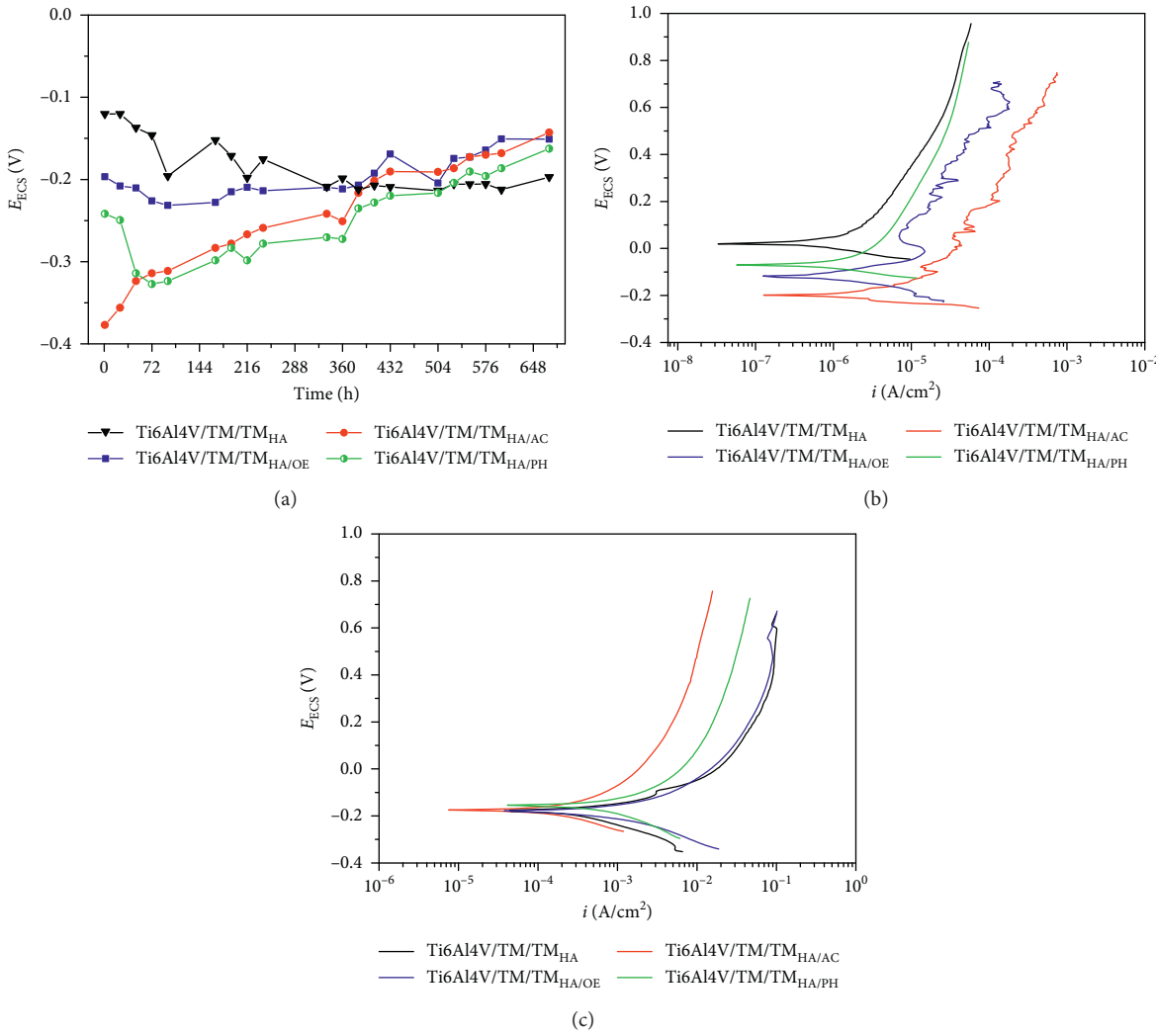

Figure 9: (a) Daily open circuit potential during 672 hours of immersion; polarization curves after (b) 1 hour and (c) 672 hours of coating immersion before and after sterilization processes in SBF at 37 ± 3°C.

the polarization curves obtained at 1 hour and 672 hours, in which the current density values increased from 10^{-6} to 10^{-4} (Figure 9(b)) and from 10^{-3} to 10^{-1} (Figure 9(c)).

After 672 hours of immersion, the sterilized coatings presented the development of less active potentials and lower current densities in the anodic sweepings when compared to the nonsterilized samples (Figure 9(c)). It evidences even more the effect of the sterilization processes on the electrochemical behavior of the samples. The degradation behavior previously observed (Figure 9(b)) most likely contributed to the increase in the permeability of the electrolyte through the coatings, leading to the formation of corrosion products on the metallic substrate, Ti6Al4V alloy [16, 52], which, consequently, caused the blockage of the surface defects and the reduction of the current density developed in the anodic sweep. In addition, the reduction of current density on the surface caused by the deposition of the apatite layer formed on the coatings, corroborating the findings on bioactivity behavior (Figures 6 and 7), can be related mainly to the Ti6Al4V/TM/TM$_{HA/AC}$ sample.

3.2.4. Wear Resistance. Figure 10 shows the evolution of the friction coefficients obtained from the ball-on-plate wear resistance test for the nonsterilized coating, and for the coatings sterilized by the different processes as a function of time.

Based on the analysis of Figure 10(a), all hybrid coatings presented similar friction coefficient values, these being similar to those obtained for the nonsterilized sample as well, with values close to $\mu = 0.7$. The rupture of the coatings was evidenced by the decrease in the coefficient of friction from $\mu = 0.7$ to $\mu = 0.55$–0.65. However, the sterilized bioactive coatings broke off in the first few seconds (50 s) of the assay, all practically at the same time, while the nonsterilized coat broke within approximately 100 seconds of assay.

Subsequently, the rupture of the protective layer can be observed with the decrease in the friction coefficient from $\mu = 0.55$–0.65 to $\mu = 0.4$. The intense oscillation of the observed value may have been due to the presence of the particles from the breaking of the films, which may have acted as a third wear body. Due to this last change in the

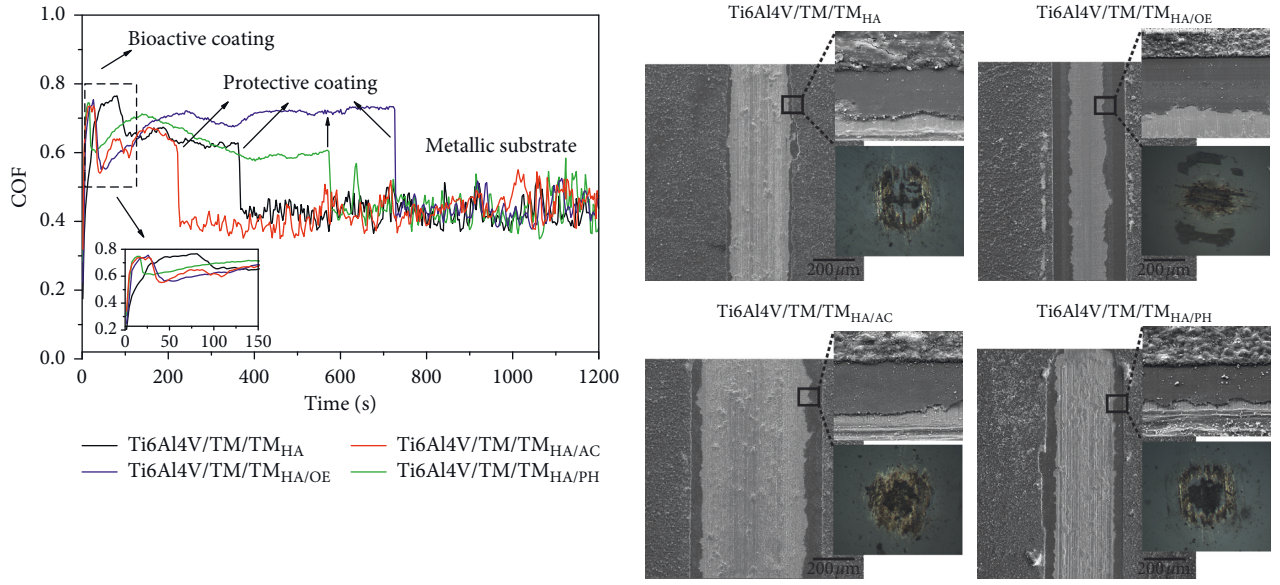

(a) (b)

Figure 10: (a) Friction coefficient of the nonsterilized and the sterilized (by three different processes) coatings as a function of time (load of 0.3 N, frequency of 1 Hz, track width of 2 mm, and counterbody = zirconia); (b) SEM/FEG micrographs of the tracks and YSZ balls after the wear tests.

friction coefficient, and its constant behavior until the end of the analysis time, the rupture of the two coatings deposited is expected. Based on this rupture, the friction coefficient could be verified as similar to that mentioned in the literature for the Ti6Al4V substrate ($\mu = 0.4$) [53, 54].

Figure 10(b) shows the images obtained in the SEM/FEG of the tracks on the coatings on which the wear tests were carried out and the YSZ balls used as a counterbody. By analyzing the micrographs of the tracks after the wear tests, the rupture of the bioactive coatings and of the underlying coatings was confirmed.

Even with the application of the bioactive coating, the wear behavior of the previously deposited protective coating was influenced by the different sterilizations. As seen in Figure 10(a), the ethylene oxide sterilized sample showed the highest rupture strength of the protective coating, followed by the hydrogen peroxide plasma and the autoclave processes. In addition, the protective coatings of the samples sterilized by ethylene oxide and by plasma of hydrogen peroxide presented higher resistance to wear than the nonsterilized coating, showing the positive influence of the sterilization methods on the mechanical properties of these coatings.

In general, the autoclaved sample (Ti6Al4V/TM/TM$_{HA/AC}$) was the one with the lowest wear resistance, evidenced by a greater track width, and a greater amount of coating material transferred to the YSZ balls, as seen in Figure 10(b). However, the ethylene oxide sterilized sample (Ti6Al4V/TM/TM$_{HA/OE}$) was the one with the highest wear resistance (narrower track width and less material transferred to the ball), even if compared to the nonsterilized sample (Figure 10(b)).

The higher wear resistance of the protective layer, when compared to the bioactive layer, may be associated with the higher cure temperature used for the protective layer (450°C), which should favor a greater crosslinking of this coating, consequently increasing its mechanical resistance. In addition, it should be considered that the addition of HA to the bioactive layer may also have contributed to impairing its mechanical resistance.

4. Conclusion

The sterilization methods evaluated promoted morphological changes in the hybrid coating, causing changes in the chemical structure of the coatings and in their bioactivity behavior. The autoclaved sample presented the highest structural chemical changes and, consequently, the highest degradability, even though it presented superior bioactive behavior in relation to the other samples.

The sterilization processes influenced the electrochemical behavior of the hybrid coating. The samples submitted to the autoclave and peroxide hydrogen plasma sterilization processes presented lower current density values than the samples sterilized with ethylene oxide.

Considering wear resistance for abrasion, the bioactive coatings that underwent the sterilization processes did not exhibit any significant difference in behavior among them; however, they presented lower wear performance in relation to the nonsterilized sample. In the case of the protective layer, only sterilization by autoclave presented a deleterious effect, rupturing before the nonsterilized sample. All other sterilization processes had a positive effect on abrasion wear resistance, and the ethylene oxide-sterilized sample showed the highest wear resistance.

Finally, based on the results obtained, it is possible to emphasize the relevance of the choice of the sterilization process since this will influence the final properties of the developing biomaterial.

Data Availability

The data used to support the findings of this study are available from the corresponding author upon request.

Conflicts of Interest

The authors declare no conflicts of interest.

Acknowledgments

The authors are grateful to CNPq (National Council for Scientific and Technological Development Project PVE 401211/2014-2), CAPES (Brazilian Federal Agency for Support and Evaluation of Graduate Education), UFRGS (Federal University of Rio Grande do Sul), UCS (University of Caxias do Sul), Esterilizare Company (RS, Brazil), and Pompéia Hospital (RS, Brazil) for their investment in and/or support for the research area.

References

[1] S. B. Goodman, Z. Yao, M. Keeney, and F. Yang, "The future of biologic coatings for orthopaedic implants," *Biomaterials*, vol. 34, no. 13, pp. 3174–3183, 2013.

[2] S. Ferraris, A. Venturello, M. Miola, A. Cochis, L. Rimondini, and S. Spriano, "Antibacterial and bioactive nanostructured titanium surfaces for bone integration," *Applied Surface Science*, vol. 311, pp. 279–291, 2014.

[3] M. Catauro, F. Bollino, and F. Papale, "Biocompatibility improvement of titanium implants by coating with hybrid materials synthesized by sol-gel technique," *Journal of Biomedical Materials Research Part A*, vol. 102, pp. 4473–4479, 2014.

[4] L. S. d. A. F. Oliveira, C. S. Oliveira, A. P. L. Machado, and F. P. Rosa, "Biomaterials com aplicação na regeneração óssea - método de análise e perspectivas futuras," *Revista de Ciências Médicas e Biológicas*, vol. 9, no. 1, pp. 37–44, 2010.

[5] P. Choudhury and D. C. Agrawal, "Sol-gel derived hydroxyapatite coatings on titanium substrates," *Surface and Coatings Technology*, vol. 206, no. 2-3, pp. 360–365, 2011.

[6] P. Dubruel, E. Vanderleyden, M. Bergadà et al., "Comparative study of silanisation reactions for the biofunctionalisation of Ti-surfaces," *Surface Science*, vol. 600, no. 12, pp. 2562–2571, 2006.

[7] J. Ballarre, I. Manjubala, W. H. Schreiner, J. C. Orellano, P. Fratzl, and S. Ceré, "Improving the osteointegration and bone-implant interface by incorporation of bioactive particles in sol-gel coatings of stainless steel implants," *Acta Biomaterialia*, vol. 6, no. 4, pp. 1601–1609, 2010.

[8] G. J. Owens, R. K. Singh, F. Foroutan et al., "Sol-gel based materials for biomedical applications," *Progress in Materials Science*, vol. 77, pp. 1–79, 2016.

[9] D. Wang and G. P. Bierwagen, "Sol-gel coatings on metals for corrosion protection," *Progress in Organic Coatings*, vol. 64, no. 4, pp. 327–338, 2009.

[10] V. Farano, J. C. Maurin, N. Attik, P. Jackson, B. Grosgogeat, and K. Gritsch, "Sol–gel bioglasses in dental and periodontal regeneration: a systematic review," *Journal of Biomedical Materials Research Part B: Applied Biomaterials*, vol. 8, pp. 1–18, 2018.

[11] R. Galante, D. Ghisleni, P. Paradiso et al., "Sterilization of silicone-based hydrogels for biomedical application using ozone gas: comparison with conventional techniques," *Materials Science and Engineering: C*, vol. 78, pp. 389–397, 2017.

[12] M. Savaris, V. d. Santos, and R. N. Brandalise, "Influence of different sterilization processes on the properties of commercial poly(lactic acid)," *Materials Science and Engineering: C*, vol. 69, pp. 661–667, 2016.

[13] M. Hirano, T. Kozuka, Y. Asano, Y. Kakuchi, H. Arai, and N. Ohtsu, "Effect of sterilization and water rinsing on cell adhesion to titanium surfaces," *Applied Surface Science*, vol. 311, pp. 498–502, 2014.

[14] J. H. Park, R. Olivares-Navarrete, R. E. Baier et al., "Effect of cleaning and sterilization on titanium implant surface properties and cellular response," *Acta Biomaterialia*, vol. 8, no. 5, pp. 1966–1975, 2012.

[15] W. Walke, Z. Paszenda, T. Pustelny et al., "Evaluation of physicochemical properties of SiO_2-coated stainless steel after sterilization," *Materials Science and Engineering: C*, vol. 63, pp. 155–163, 2016.

[16] E. K. K. Baldin, C. Garcia, J. A. P. Henriques et al., "Effect of sterilization processes on the properties of a silane hybrid coating applied to Ti6Al4V alloy," *Journal of Materials Research*, vol. 33, no. 2, pp. 161–177, 2018.

[17] M. Wang, Y. Wang, Y. Chen, and H. Gu, "Improving endothelialization on 316L stainless steel through wettability controllable coating by sol-gel technology," *Applied Surface Science*, vol. 268, pp. 73–78, 2013.

[18] J. Ballarre, D. A. López, W. H. Schreiner, A. Durán, and S. M. Ceré, "Protective hybrid sol-gel coatings containing bioactive particles on surgical grade stainless steel: surface characterization," *Applied Surface Science*, vol. 253, no. 17, pp. 7260–7264, 2007.

[19] J. Ballarre, R. Seltzer, E. Mendoza et al., "Morphologic and nanomechanical characterization of bone tissue growth around bioactive sol-gel coatings containing wollastonite particles applied on stainless steel implants," *Materials Science and Engineering: C*, vol. 31, no. 3, pp. 545–552, 2011.

[20] C. García, S. Ceré, and A. Durán, "Bioactive coatings prepared by sol-gel on stainless steel 316L," *Journal of Non-Crystalline Solids*, vol. 348, pp. 218–224, 2004.

[21] S. Omar, F. Repp, P. M. Desimone et al., "Sol-gel hybrid coatings with strontium-doped 45S5 glass particles for enhancing the performance of stainless steel implants: electrochemical, bioactive and in vivo response," *Journal of Non-Crystalline Solids*, vol. 425, pp. 1–10, 2015.

[22] T. Kokubo and H. Takadama, "How useful is SBF in predicting in vivo bone bioactivity?," *Biomaterials*, vol. 27, no. 15, pp. 2907–2915, 2006.

[23] A. Zomorodian, F. Brusciotti, A. Fernandes et al., "Anticorrosion performance of a new silane coating for corrosion protection of AZ31 magnesium alloy in Hank's solution," *Surface and Coatings Technology*, vol. 206, no. 21, pp. 4368–4375, 2012.

[24] L. E. Amato, D. A. López, P. G. Galliano, and S. M. Ceré, "Electrochemical characterization of sol-gel hybrid coatings in cobalt-based alloys for orthopaedic implants," *Materials Letters*, vol. 59, no. 16, pp. 2026–2031, 2005.

[25] R. Al-Oweini and H. El-Rassy, "Synthesis and characterization by FTIR spectroscopy of silica aerogels prepared using several $Si(OR)_4$ and $R''Si(OR')_3$ precursors," *Journal of Molecular Structure*, vol. 919, no. 1–3, pp. 140–145, 2009.

[26] I. M. Martínez, L. Meseguer-Olmo, A. Bernabeu-Esclapez, P. A. Velásquez, and P. N. De-Aza, "*In vitro* behavior of α-tricalcion phosphate doped with dicalcium silicate in the

system Ca_2SiO_4-$Ca_3(PO_4)_2$," *Materials Characterization*, vol. 63, pp. 47–55, 2012.

[27] R. Rojaee, M. Fathi, and K. Raeissi, "Electrophoretic deposition of nanostructured hydroxyapatite coating on AZ91 magnesium alloy implants with different surface treatments," *Applied Surface Science*, vol. 285, pp. 664–673, 2013.

[28] X. Wang, G. Song, and T. Lou, "Fabrication and characterization of nano-composite scaffold of PLLA/silane modified hydroxyapatite," *Medical Engineering & Physics*, vol. 32, no. 4, pp. 391–397, 2010.

[29] S. Rakmae, Y. Ruksakulpiwat, W. Sutapun, and N. Suppakarn, "Effect of silane coupling agent treated bovine bone based carbonated hydroxyapatite on in vitro degradation behavior and bioactivity of PLA composites," *Materials Science and Engineering: C*, vol. 32, no. 6, pp. 1428–1436, 2012.

[30] S. Rehman, K. Khan, M. Mujahid, and S. Nosheen, "Synthesis of nano-hydroxyapatite and its rapid mediated surface functionalization by silane coupling agent," *Materials Science and Engineering: C*, vol. 58, pp. 675–681, 2016.

[31] L. V. Mora, A. Taylor, S. Paul et al., "Impact of silica nanoparticles on the morphology and mechanical properties of sol-gel derived coatings," *Surface and Coatings Technology*, vol. 342, pp. 48–56, 2018.

[32] M. Hernández-Escolano, X. Ramis, A. Jiménez-Morales, M. Juan-Díaz, and J. Suay, "Study of the thermal degradation of bioactive sol-gel coatings for the optimization of its curing process," *Journal of Thermal Analysis and Calorimetry*, vol. 107, no. 2, pp. 499–508, 2012.

[33] S. M. Latifi, M. Fathi, J. Varshosaz, and N. Ghochaghi, "Simultaneous structural and surface modifications of nanophase hydroxyapatite for improving its dissolution and bioactivity," *Ceramics International*, vol. 42, no. 5, pp. 6355–6359, 2016.

[34] C. Covarrubias, M. Mattmann, A. Von Marttens et al., "Osseointegration properties of titanium dental implants modified with a nanostructured coating based on ordered porous silica and bioactive glass nanoparticles," *Applied Surface Science*, vol. 363, pp. 286–295, 2016.

[35] S. Fleith, A. Ponche, R. Bareille, J. Amédée, and M. Nardin, "Effect of several sterilisation techniques on homogeneous self assembled monolayers," *Colloids and Surfaces B: Biointerfaces*, vol. 44, no. 1, pp. 15–24, 2005.

[36] G. Wittenburg, G. Lauer, S. Oswald, D. Labudde, and C. M. Franz, "Nanoscale topographic changes on sterilized glass surfaces affect cell adhesion and spreading," *Journal of Biomedical Materials Research Part A*, vol. 102, no. 8, pp. 2755–2766, 2014.

[37] A. Han, J. K. H. Tsoi, J. P. Matinlinna, Y. Zhang, and Z. Chen, "Effects of different sterilization methods on surface characteristics and biofilm formation on zirconia in vitro," *Dental Materials*, vol. 34, no. 2, pp. 272–281, 2018.

[38] M. Pegueroles, F. J. Gil, J. A. Planell, and C. Aparicio, "The influence of blasting and sterilization on static and time-related wettability and surface-energy properties of titanium surfaces," *Surface and Coatings Technology*, vol. 202, no. 15, pp. 3470–3479, 2008.

[39] F. Variola, J.-H. Yi, L. Richert, J. D. Wuest, F. Rosei, and A. Nanci, "Tailoring the surface properties of Ti6Al4V by controlled chemical oxidation," *Biomaterials*, vol. 29, no. 10, pp. 1285–1298, 2008.

[40] O. Bareiro and L. A. Santos, "Tetraethylorthosilicate (TEOS) applied in the surface modification of hydroxyapatite to develop polydimethylsiloxane/hydroxyapatite composites," *Colloids and Surfaces B: Biointerfaces*, vol. 115, pp. 400–405, 2014.

[41] T. Tański, W. Matysiak, Ł. Krzemiński, P. Jarka, and K. Gołombek, "Optical properties of thin fibrous PVP/SiO_2 composite mats prepared via the sol-gel and electrospinning methods," *Applied Surface Science*, vol. 424, pp. 184–189, 2017.

[42] X. Wang, F. Liu, and Y. Song, "Enhanced corrosion resistance and in vitro bioactivity of NiTi alloys modified with hydroxyapatite-containing Al_2O_3 coatings," *Surface and Coatings Technology*, vol. 344, pp. 288–294, 2018.

[43] E. C. S. Rigo, A. O. Boschi, M. Yoshimoto, S. Allegrini, B. Konig, and M. J. Carbonari, "Evaluation in vitro and in vivo of biomimetic hydroxyapatite coated on titanium dental implants," *Materials Science and Engineering: C*, vol. 24, no. 5, pp. 647–651, 2004.

[44] R. A. Surmenev, M. A. Surmeneva, and A. A. Ivanova, "Significance of calcium phosphate coatings for the enhancement of new bone osteogenesis-a review," *Acta Biomaterialia*, vol. 10, no. 2, pp. 557–579, 2014.

[45] N. Khoshnood, A. Zamanian, and A. Massoudi, "Effect of silane-coupling modification on bioactivity and in vitro properties of anodized titania nanotube arrays," *Materials Letters*, vol. 185, pp. 374–378, 2016.

[46] C. Y. Zheng, F. L. Nie, Y. F. Zheng et al., "Enhanced corrosion resistance and cellular behavior of ultrafine-grained biomedical NiTi alloy with a novel SrO–SiO_2–TiO_2 sol–gel coating," *Applied Surface Science*, vol. 257, no. 3, pp. 5913–5918, 2011.

[47] G. Tan, K. Ouyang, H. Wang et al., "Effect of amino-, methyl- and epoxy-silane coupling as a molecular bridge for formatting a biomimetic hydroxyapatite coating on titanium by electrochemical deposition," *Journal of Materials Science & Technology*, vol. 32, no. 9, pp. 956–965, 2016.

[48] S. Heise, T. Wirth, M. Höhlinger et al., "Electrophoretic deposition of chitosan/bioactive glass/silica coatings on stainless steel and WE43 Mg alloy substrates," *Surface and Coatings Technology*, vol. 344, pp. 553–563, 2018.

[49] M. M. Ibañez, I. Aldalur, F. J. Romero-Gavilán, J. Suay, I. Goñi, and M. Gurruchaga, "Designs of nanostructured siloxane-gelatin coatings: immobilization strategies and dissolution properties," *Journal of Non-Crystalline Solids*, vol. 481, pp. 368–374, 2018.

[50] M. Araújo, M. Miola, A. Venturello, G. Baldi, J. Pérez, and E. Verné, "Glass coatings on zirconia with enhanced bioactivity," *Journal of the European Ceramic Society*, vol. 36, no. 13, pp. 3201–3210, 2016.

[51] S. M. Hosseinalipour, A. Ershad-langroudi, A. N. Hayati, and A. M. Nabizade-Haghighi, "Characterization of sol-gel coated 316L stainless steel for biomedical applications," *Progress in Organic Coatings*, vol. 67, no. 4, pp. 371–374, 2010.

[52] M. Basiaga, W. Walke, Z. Paszenda, and A. Kajzer, "The effect of EO and steam sterilization on the mechanical and electrochemical properties of titanium Grade 4," *Materiali in tehnologije*, vol. 50, no. 1, pp. 153–158, 2016.

[53] M. Buciumeanu, A. Araujo, O. Carvalho et al., "Study of the tribocorrosion behaviour of Ti6Al4V-HA biocomposites," *Tribology International*, vol. 107, pp. 77–84, 2017.

[54] F. Bartolomeu, M. Buciumeanu, E. Pinto et al., "Wear behavior of Ti6Al4V biomedical alloys processed by selective laser melting, hot pressing and conventional casting," *Transactions of Nonferrous Metals Society of China*, vol. 27, no. 4, pp. 829–838, 2017.